Gyroid-Structured 3D ZnO Networks Made by Atomic Layer Deposition

Ellie Kim[1], Yana Vaynzof[1], Alessandro Sepe[1], Stefan Guldin[1,†], Maik Scherer[1], Pedro Cunha[1], Stephan V. Roth[2], & Ullrich Steiner[1*]

3D continuous ZnO morphologies with characteristic feature sizes on the 10-nm lenght scale are attractive for electronic device manufacture. Their synthesis remains however a challenge because of the low crystalisation temperature of ZnO. Here, we report a method for the robust and reliable synthesis of fully crystalline 3D mesoporous ZnO networks by means of atomic layer deposition (ALD) of ZnO into a self-assembled block copolymer template. By carefully optimising the the processing conditions we are able to synthesise several micrometer thick layers of mesoporous ZnO networks with a strut-width of ∼30 nm. Two 3D mesoporous morphologies were manufactured: a periodic gyroid structure and a random wormlike morphology. Exploiting the ALD property to conformally coat complex surfaces of high aspect ratios, the channel network of a 3D continous channel network of a self-assembled block copolymer was replicated into ZnO. X-ray photoemission spectroscopy (XPS) and x-ray diffraction measurements reveal that the chemical composition of the mesoporous structures is uniform and consists of wurtzite-ZnO throughout the film. Scanning electron microscopy (SEM) reveals an average pore dimension of ≈30 nm.The potential of this material for a hybrid photovoltaic application is demonstrated by the manufacture of a poly(3-hexylthiophene)/ZnO solar cell.

[1]Cavendish Laboratory, Department of Physics, University of Cambridge, J. J. Thomson Avenue, Cambridge CB3 0HE, UK. [2]HASYLAB at DESY, Notkestr. 85, 22607 Hamburg, Germany. [†]Now at: Supramolecular Nano-Materials and Interfaces Laboratory, Department of Materials Science, École Polytechnique Fédérale de Lausanne, 1015 Lausanne, Switzerland. [*]e-mail: u.steiner@phy.cam.ac.uk

1 Introduction

ZnO is a direct semiconductor with a wide bandgap of 3.37 eV with piezoelectric, photocatalytic, and gas sensing properties.[1] In its thin film form, it is used as a transparent (semi)conductive electrode for optoelctronic and solar cell applications.[2] Three-dimensional, porous structures of ZnO have been of technological interest in emerging areas of nanotechnology as they offer opportunities for applications that require a high surface area or hybrid materials.

Unlike other transition metal oxides such as TiO_2, and SnO_2 and despite equally desirable properties, ZnO is very difficult to process into well-defined morphologies on the sub-100 nm length scale. Instead of well defined 3D structures that are possible with other metal oxides[3] 1D ZnO morphologies can be produced *via* anisotropic growth to form nanorods, nanowires, nano coils, and nano-forests.[4–6] The difference to the other metal oxides lies in the rapid crystallization of ZnO from solution. In contrast to for example TiO_2, which is amorphous during room-temperature deposition and crystallizes only upon heating, ZnO crystallization sets in at room temperature. Therefore, attempts to mould ZnO into design structures using sol-gel or electrodeposition methods have been unsuccessful, because structure formation is governed by ZnO crystallization and not the mould. Reports on porous ZnO structures using such methods showed the replication of pore sizes larger than 200 nm[7] or poorly defined morphologies[8,9]

In this work, the problems of rapid crystallization during deposition was circumvented by the use of atomic layer deposition (ALD) to replicate a periodic and random 3D networks generated by the microphase separation of a blockcopolymer (BCP). This enables the fabrication of 3D continuous structures of ZnO with feature sizes below 50 nm and controllable layer thicknesses ranging from 200 nm to several microns.

BCPs self-assemble into well-defined morphologies with tunable feature sizes ranging between 10-100 nm. The resulting morphologies are governed mainly by the molecular architecture of the blockcopolymer, with spherical, cylindrical and lamellar arrays being most commonly obtained in diblock copolymers. The more elusive double gyroid morphology is a particularly appealing candidate for the manufacture of 3D bicontinuous nanostructured templates. The double gyroid consists of two interwoven, periodic, continuous networks of the minority block surrounded by a matrix of the majority block.[10] It provides a useful template for the replication of self-supporting 10-nm scaffolds of

metals and metal oxides, which have been employed in the manufacture of dye-sensitized solar cells, electrochromic devices, and supercapacitors.

While the self-assembly of BCPs into the gyroid phase is often challenging and slow, a faster and more robust use of BCP self-assembly employs off-equilibrium morphologies. Cylinder and gyroid-forming BCPs are often observed to form 3D interconnected bicontinuous wormlike morphologies when quenched off equilibrium[11]. Although less periodic, the formation of wormlike structures in thin films with bicontinuous micro phases is simpler and more robust compared to the equilibration into the gyroid morphology. These non-equilibrium structures are therefore good candidates for the scalable synthesis of functional nanomaterials.

BCP self-assembly has been used to pattern metal oxides either by the co-assembly of a precursor sol[12] and as a sacrificial template for metal and metal oxide electrodeposition[3] and solution impregnation[13].

ALD is a precise chemical vapor deposition technique for the three dimensional, conformal replication of a scaffold in a highly controlled manner. Successful 3D deposition requires however a careful optimization of processing parameters such as exposure time to the precursor gases, precursor partial pressure, and deposition temperature, all of which have to be adjusted to the aspect ratio and surface chemistry of the porous substrates. Several models and simulation methods have been suggested to describe conformal deposition onto very high aspect ratio (>10000) substrates, such as alumina membranes (AAO), nanotubes, or inverse opals.[14–16] Wang *et al.* reported the deposition of ZnO onto a complex polymer structure of tubular shape.[17] Despite this early work, the replication of BCP templates by ALD to yield a 3D metal oxide structure has remained a considerable challenge.

The purpose of this study is the demonstration of a method for the manufacture of 3D continuous mesoporous ZnO network structures by replicating a self-assembled polymer substrate using the ALD, exploiting the advantages of both methodologies. Starting with a porous template obtained by BCP self-assembly followed by the selective etching of one of the polymer phases, ZnO was conformally deposited by ALD, replicating the complex 3D high aspect ratio gyroid internal surfaces by ZnO. The use of this material in a solar cell is demonstrated.

2 Results and Discussion

2.1 Mesoporous ZnO preparation

2.1.1 Polymer templates

Figure 1 demonstrates the sample preparation procedure. Periodic gyroid and random wormlike structured films were fabricated from the same polymer solution, a mixture of a lamellae-forming polystyrene-polyisoprene (PS-PI) blockcopolymer and PS homopolymer.[18,19] The ratio of the two polymers was finely adjusted to an overall PS volume fraction of 65%, which is a requirement for the formation of the double gyroid phase.

The double gyroid morphology was obtained by carefully annealing the film into its narrowly defined phase equilibrium, which requires a slow solvent evaporation process. The wormlike structure is, on the other hand, readily obtained by quenching the film by spin-coating, which yields a morphology that is far from thermodynamic equilibrium.

Both template systems have distinct benefits. The gyroid morphology provides a highly ordered, periodic 3D structure. Its manufacture by drop-casting and slow solvent annealing remains however a challenge. The thickness of the polymer template can be roughly controlled by varying the concentration of the deposition solution, yielding values between 2-8 µm.

The wormlike morphology, on the other hand, is not as periodic as the gyroid. It nevertheless provides a well-defined bicontinuous porous morphology. (Fig. 1) The processing conditions are easy and quick (∼15 hours) compared to those based on the gyroid templates (> 8 days) and the resulting films are of consistent smoothness and thickness. By varying the polymer solution concentration and the spin-coating conditions, controlled thickness between 200 nm and 3 µm were obtained.

For both systems, upon complete evaporation of the solvent, the PI block was removed to provide a porous network of pores for the deposition of ZnO. To this end, the polymer film was exposed to UV (254 nm) and immersed in ethanol for up to 15 hours, resulting in the 3D porous polystyrene structure as shown in Fig. 2a and Fig. 3a.[18,19] The UV exposure not only breaks down the backbone of the PI, it also creates carboxylic groups on the PS.[20] Thus, upon ethanol immersion, the PS surface is terminated by OH groups, which is an important requirement for the conformal ALD deposition of ZnO.

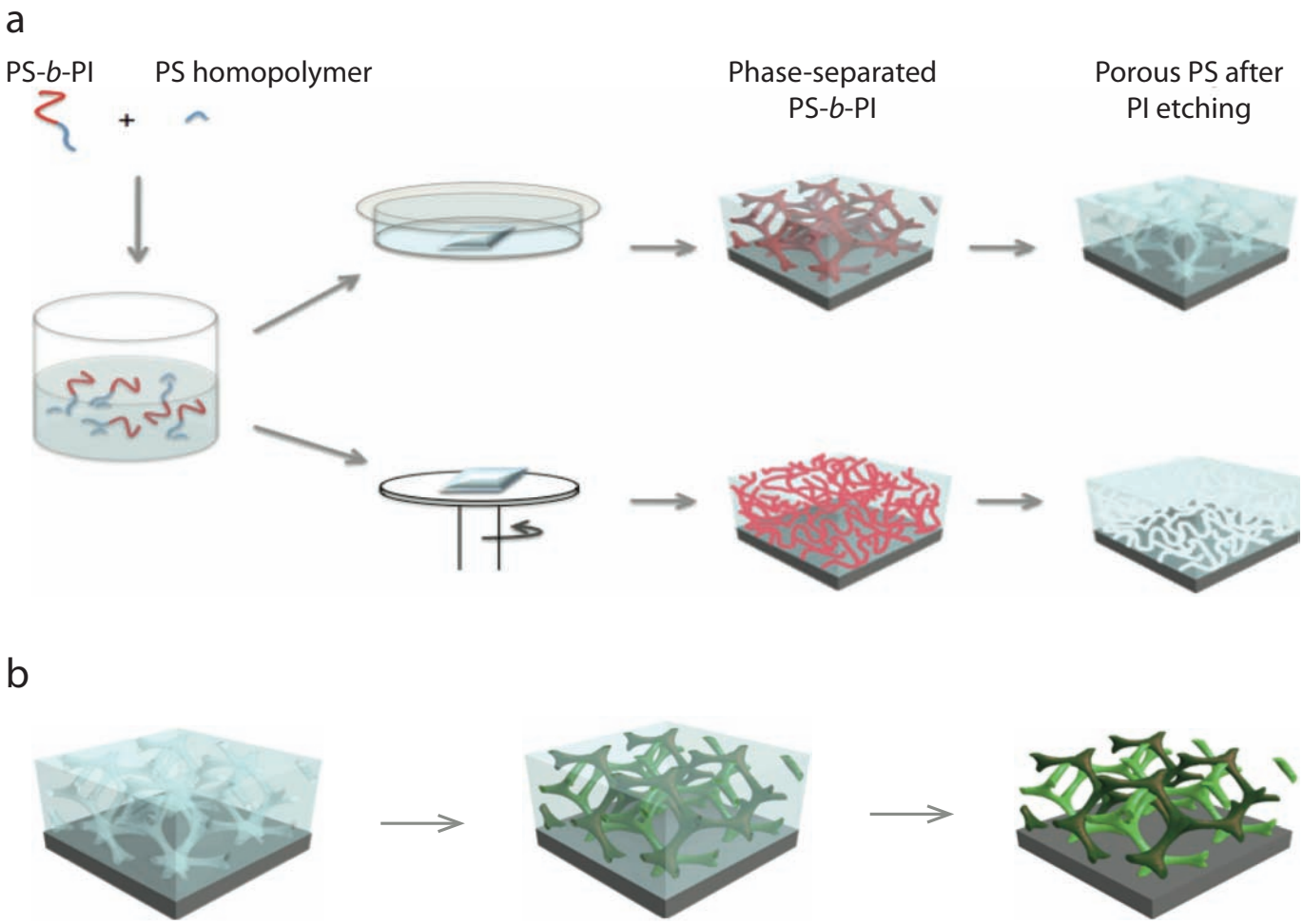

Figure 1: Schematic representation of the sample preparation procedure. (a) A porous PS template is created by BCP phase separation followed by selective PI etching. (b) ALD replication of the polymer template by ZnO.

2.1.2 ALD deposition of ZnO onto a mesoporous PS template

The steps of the replication process in Fig. 1b are demonstrated in the scanning electron microscope (SEM) images of Fig. 2a-c and Fig. 3a-c. ZnO was ALD-deposited using diethyl zinc (DEZ) and H_2O precursors onto the template, followed by removal of the polymer. The ZnO-polymer hybrid (before removal of the polymer) is shown in Fig. 2b. The polymer template and the area where not sufficient ZnO was deposited appear dark in the SEM images because of charging of the non-conductive PS template.

ALD deposition into polymer templates requires the careful selection of the deposition temperature. The ALD deposition window for ZnO is 80 - 150 °C, delimited by the minimum precursor reaction temperature and the precursor desorption from the template walls.[21] PS has a glass transition temperature of ≈ 100 °C. To test the softening temperature of the cross-linked self-assembled PS templates they were annealed for 24 h at temperatures up to 120 °C. The cross-linked polymer template was found to withstand up to 110°C, above which deformation of morphology and collapse of the polymer structure was observed. In order to keep this method applicable for other different types of polymer templates, the default deposition temperature was kept at 80 °C, the lowest possible of the conformal deposition window. The 100 °C deposition was later investigated to explore the deposition temperature dependence of crystallite size of deposited ZnO, but the crystallite size did not differ from that of 80 °C deposition (Fig. 6b).

The diameter of the void channels running through the polymeric template was roughly 32 nm for gyroid, and 25-35 nm for the wormlike structure. Given that the growth rate of ZnO is approximately 1.5 Å- 2.2 Å/cycle,[7,22] 110 cycles of ZnO were deposited in order to aim for a minimum of 16.5 nm deposition on the template surface, which under the assumption of conformal coating should completely fill the voided network. The thin solid layer of ∼20 nm

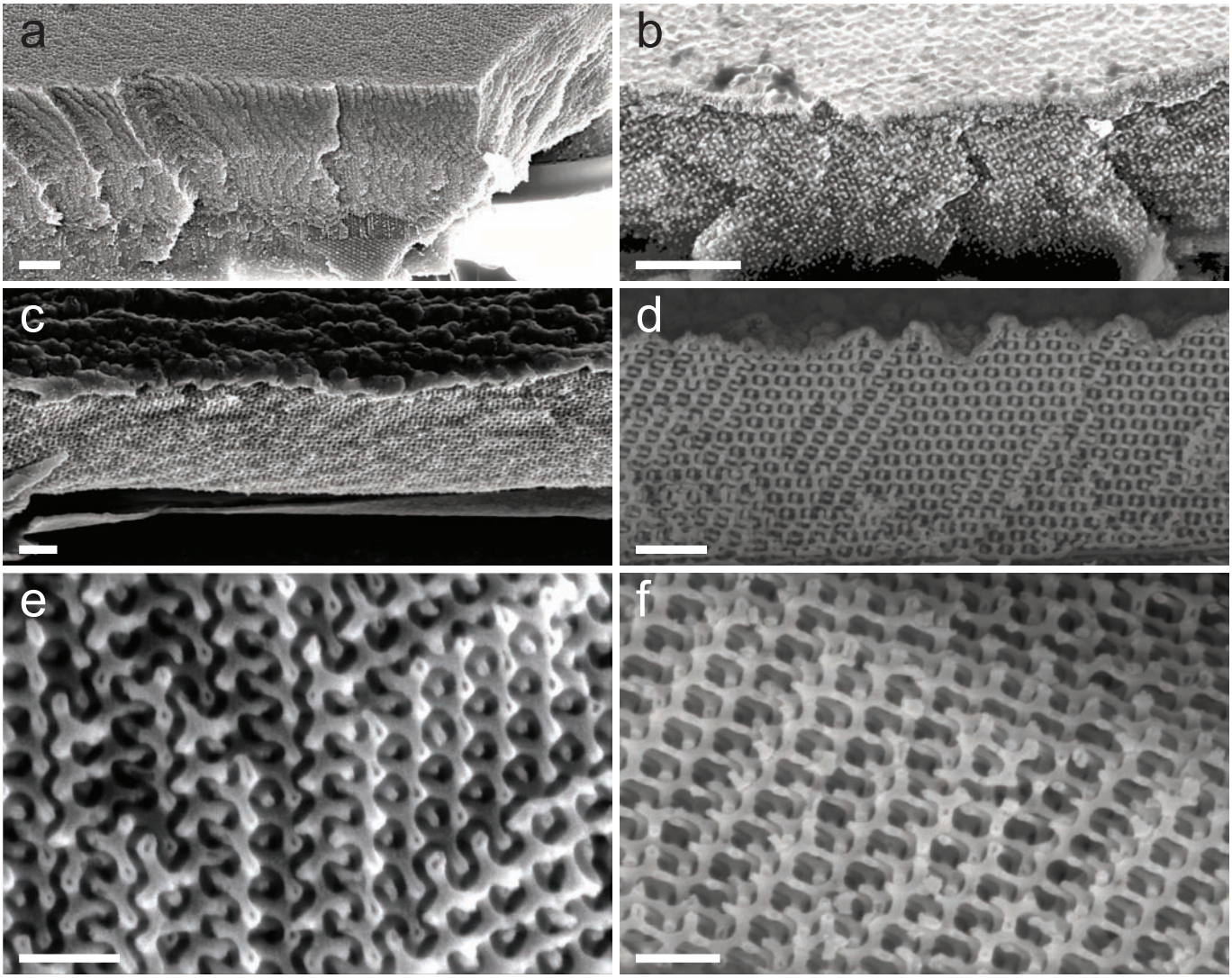

Figure 2: Side-view SEM images at a 45° angle of gyroid replication into ZnO. (a) Gyroid polystyrene template (b) as deposited ZnO-PS hybrid (c) ZnO gyroid after annealing at 550 °C. (d), (e), (f) show different faces of ZnO gyroid of (c). The scale bars correspond to 1 µm for (a) and (b), 400 nm for (c) and (d), 200 nm for (e) and (f).

that has formed on top of the porous film results from the surface limited, conformal deposition, which can easily be removed using dry etching methods such as reactive ion etching (RIE) or inductive coupled plasma etching (ICP).

After removal of the PS matrix by heating the sample to 400 °C or by exposure to a oxygen plasma, free-standing ZnO networks are revealed. The replicated ZnO gyroid film is self-standing and highly periodic with a consistent channel diameter of approximately 30 nm. Figure 2d-f shows other lattice faces of the gyroid ZnO structure imaged from different angles. The wormlike structure was similarly replicated using ALD, fabricating 3D bicontinuous ZnO replica with film thicknesses of 200 nm - 2 µm (Fig. 3a,c). The similar quality of the replicated networks in Figs. 2 and 3 proves that the wormlike polymer template has a similar pore connectivity as the double gyroid. Both ZnO structures were annealed at temperatures between 400 °C and 550 °C, demonstrating the stability of both network types in this temperature range. The stability of the ZnO mesomorphology at temperatures above the complete degradation of PS (between 300°C and 400°C) mirrors the good structural integrity observed in other metal-oxide mesomorphologies.[23]

The successful replication of the ZnO networks in Figs. 2 and 3 required the careful optimization of ALD parameters. Two types of exposure methods were explored, the continuous flow and stop-flow methods, described by Karuturi *et al.*[15] The exposure times required for successful replication were comparable to what has been reported for high aspect ratio structures: 30 s to 2 min for each pulse and purge step and 10 - 20 s exposure with hold times between 1-4 min, for

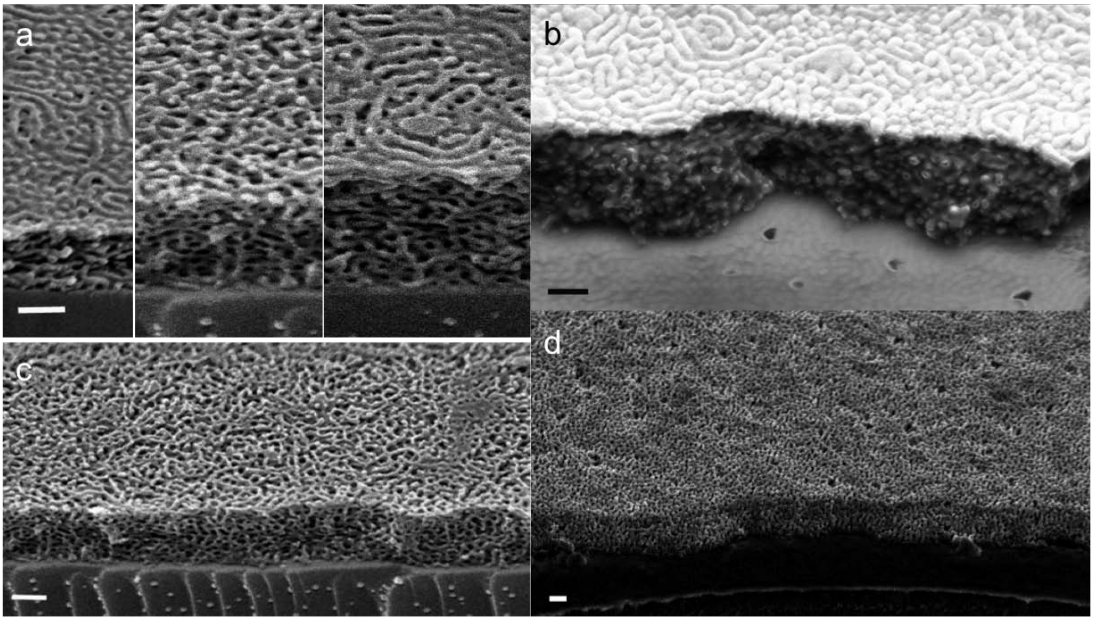

Figure 3: SEM of ZnO replication of the wormlike morphology. (a), (c) wormlike polystyrene template, (b) as deposited ZnO-PS hybrid, and (d) ZnO morphology after annealing at 400 °C followed by ICP etching of the top compact layer. All scale bars are 200 nm.

the two methods, respectively. While both methods successfully replicated the 3D network morphology, the stop-flow method was more practical because pulsing the precursors for up to 2 minutes per cycle had a precursor consumption of up to 240 min per sample, whereas the stop-flow method only required 20-40 min precursor consumption time, while exposing the template to the precursor for a similar time period as in the continuous flow method. The ALD parameters of the samples shown in the figures are summarized in Table 1.

Sample	No. of Cycles	DEZ Pulse	Hold	Purge	H_2O Pulse	Hold	Purge
Fig. 2, Fig. 4	1-30	30 s	- -	30 s	30 s	- -	30 s
	31-60	30 s	30 s	30 s	30 s	30 s	30 s
	61-90	30 s	1 min 30 s	1 min 30 s	30 s	1 min 30 s	1 min 30 s
	91-110	30 s	2 min 30 s	2 min 30 s	30 s	2 min 30 s	2 min 30 s
Fig. 3, Fig. 5	1-30	15 s	45 s	1 min	15 s	45 s	1min
	31-60	15 s	1 min 30 s	1 min 30 s	15 s	1 min	1 min
	61-75	15 s	2 min 30 s	2 min 30 s	15 s	2 min 30 s	2 min 30 s

Table 1: Summary of the ALD parameters used to fabricate the samples shown in the figures

The careful analysis of Fig. 2 reveals the details of ALD replication. Annealing above 400 °C or O_2 plasma treatment removed polymer network revealing gyroid or worm-like ZnO morphology. In the cases when ALD deposition did not extend down to the substrate (Fig. 2b), polymer removal did not destroy the replica which settled onto the substrate fully preserving the template imposed morphology (Fig. 2c). Further evidence for incomplete ALD replication can be seen in Fig. 2e. Close to the substrate, the network struts are voided (void diameter < 5 nm) indicating that the pores near the free surface have closed before the ALD process further down was complete. Incomplete penetration of ZnO through the entire depth of the template is a consequence of the ALD parameters, including the precursor partial pressure, the exposure time, the template aspect ratio, and the chemistry of the template surface.[14,24] In addition, sufficient purge time for each half-cycle is crucial for the the removal of the unreacted precursor and the reaction byproducts

The interplay of these parameters has been experimentally and theoretically studied in high aspect ratio systems with typically > 100 nm pore widths,[14–16] often observing pore blocking and non-uniform coatings.[25] The present system differs however from 1D model architectures. Our 3D bicontinuous networks have more complex morphologies of interconnected channels. The high specific surface area (compared to 1D channels) may require longer pulse and purge

times to achieve complete saturation of the substrate surface and removal of the reaction products.[14–16] Furthermore, the small feature size of ~ 30 nm may complicate the control of ZnO crystallization. A confinement diameter that is comparable to the size of a critical nucleation seed may either inhibit ZnO crystallization or cause pore blockage by uncontrolled crystal nucleation. The latter is confirmed by XRD results, observing 8 nm ZnO crystallites in the as-deposited gyroid matrix (see below).

Crystallite or cluster formation is enhanced for surfaces which are only sparsely covered by groups that can react with the ALD precursor. For the diethyl zinc precursor used in this study, a dense surface coverage of the polymer scaffold by OH groups is therefore essential.[26] In the PS-PI self-assembled template, OH and COOH groups are created during UV exposure, which also degrades the PI.[20] The SEM image shown in Fig. 5 confirms the formation of a uniform initial coating and the absence of cluster formation on the 10-nm length scale.

Void formation in Fig. 2 was insensitive to changes in the ALD cycle parameters (e.g. an increase in the exposure duration by a factor of 2). Careful analysis of Fig. 5 shows that the pores at the top of the film have closed after ≈ 65 cycles (rather than the calculated 80-90 cycles) assuming true atomic layer deposition, this corresponds to a deposition of 10-15 nm, leaving a 3-7 nm core unfilled. We propose two possible reasons for the incomplete pore filling of Fig. 2. Firstly, the long exposure time to the ALD precursor which is necessary because of the large aspect ratio of the network may result in multilayer adsorption in the pores close to the surface and therefore more rapid ZnO Layer growth. Secondly, the degradation of PI with UV light is less efficient deeper inside the film (up to 48 h UV exposure followed by 48 h ethanol dissolution are reportedly required to completely remove the PI[27]). This may result in incomplete degradation and/or alteration of the surface chemistry and therefore an incomplete ALD process. Nevertheless, ALD infiltration into up to 5 µm thick templates was achieved (Fig. 4).

2.1.3 Deposition temperature

The long cycle times required by the high aspect ratio pores result in stringent requirements concerning the temperature stability of the polymer matrix. This was assessed by annealing the templates in vacuum for up to 24 hours in temperatures up to 120 °C. The cross-linked PS morphology was found to withstand up to 110 °C, above which a collapse of the polymer structure was observed. This lies well within the temperature window for ALD ZnO deposition of 80 °C-150 °C,[21] which is limited by a lack of surface reactivity (low T) and precursor dissociation. The lowest possible deposition temperature was therefor chosen. A higher temperature of 100 °C yielded very similar results (Fig. 6b).

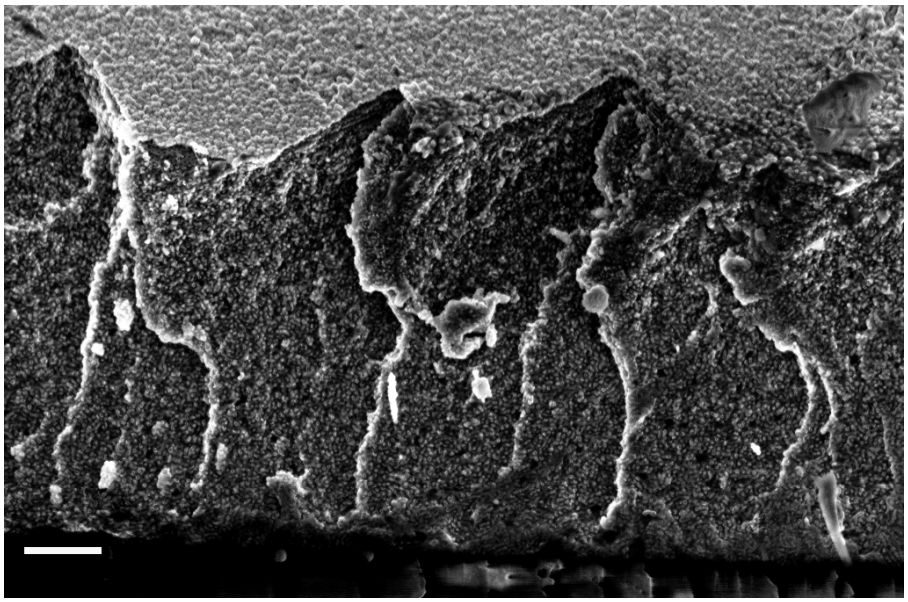

Figure 4: Cross sectional SEM image of wormlike ZnO-PS hybrid. ZnO was deposited conformally onto a ~ 5 µm-thick wormlike PS template. The scale bar corresponds to 1 µm.

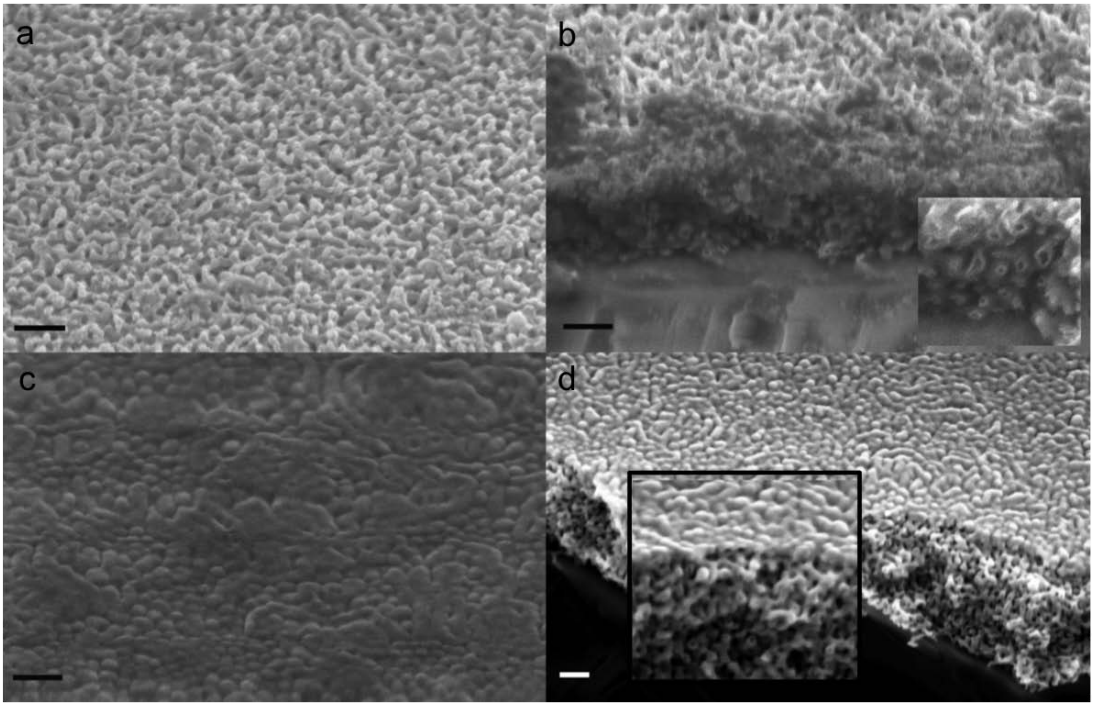

Figure 5: ALD deposited ZnO replica of porous polymer templates. (a) Top layer (b) cross section after 30 cycles and (c), (d) after 75 cycles. The scale bars are 200 nm.

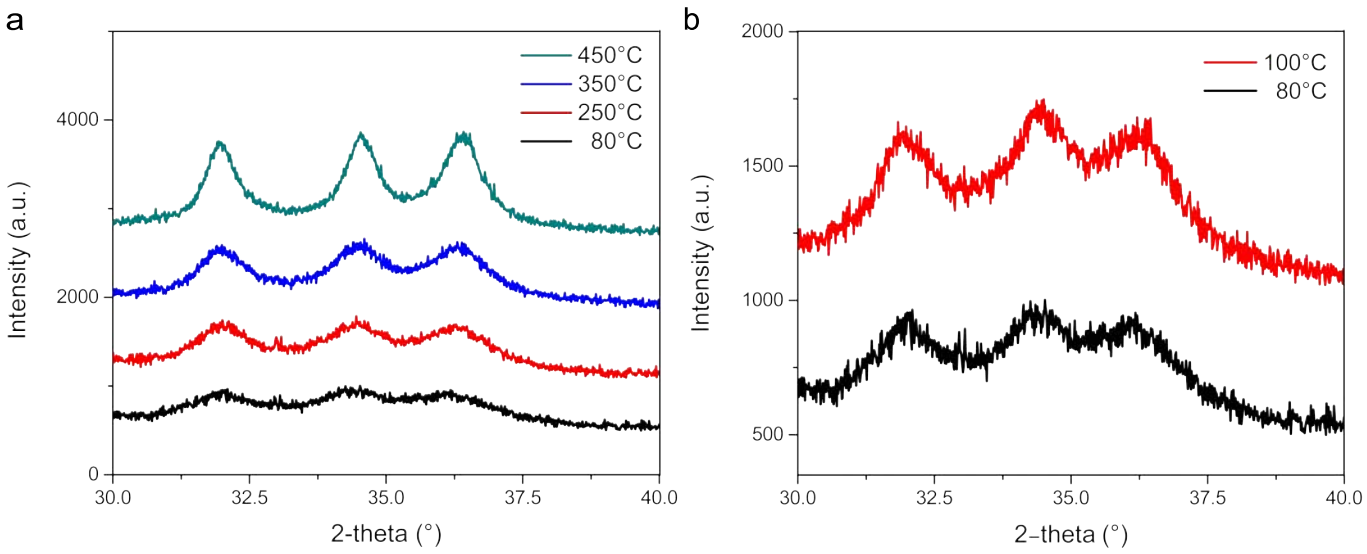

Figure 6: WAXS characterization of mesoporous ZnO. (a) Effect of post thermal annealing after ALD deposition at 80 °C. (b) As deposited without further annealing.

2.1.4 Characterization by X-ray diffraction

The replicated ZnO was characterized by wide-angle x-ray scattering (WAXS) to examine ZnO crystallization as a function of the post-deposition annealing temperature. Figure 6a shows spectra of films annealed at 250 °C, 350 °C, and 450 °C. Before annealing, the polymer was removed by a O_2 plasma treatment. The peaks in the spectra correspond to wurtzite ZnO.[28] While the as-deposited film has the clear signature of ZnO crystallinity, the peaks are broad, indicating very small crystallites and possibly some amorphous content. The initial ZnO crystallinity does not depend

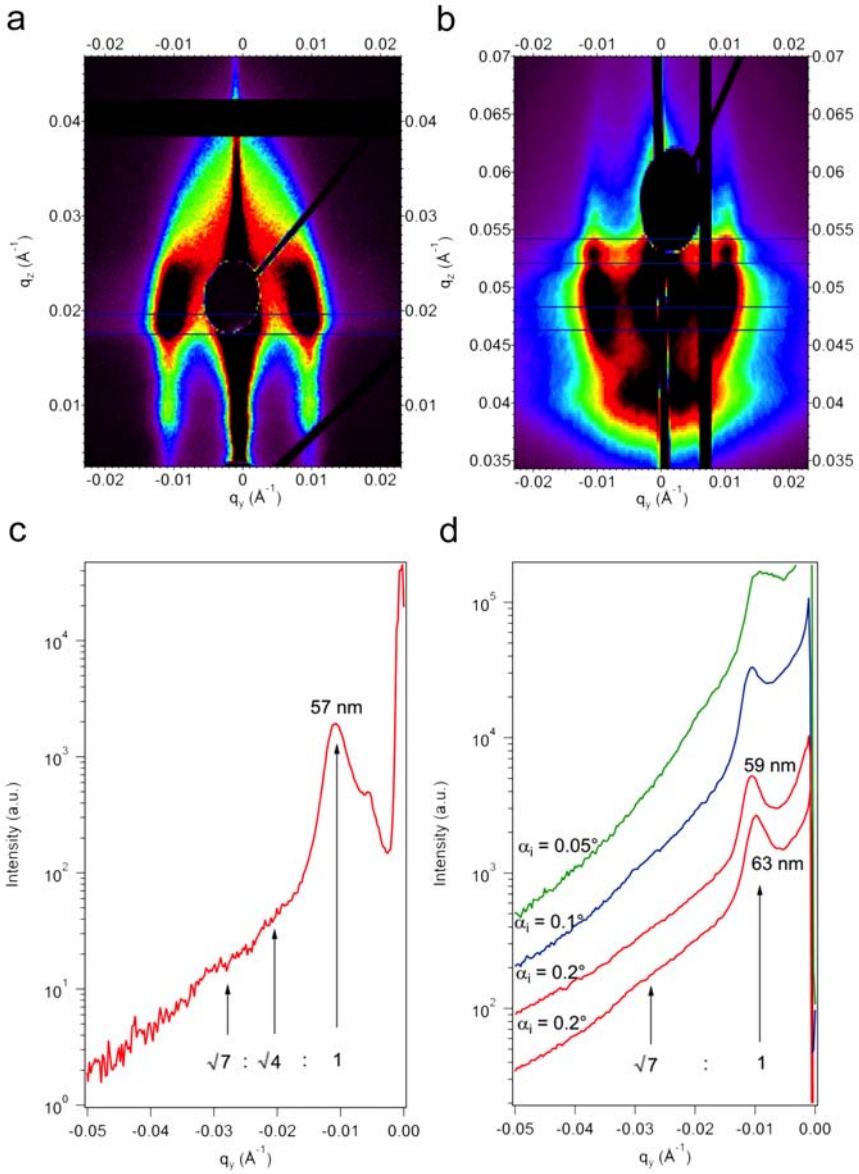

Figure 7: (a) GISAXS pattern of the wormlike polystyrene template film showing bent Bragg rods, taken at an incident angle of 0.185°. (c) Corresponding 1D GISAXS intensity profile along q_y. (b) GISAXS pattern of the resulting ZnO film after annealing at 450 °C followed by ICP etching of the top compact layer, taken at and angle of incidence of 0.2°. (d) Corresponding 1D GISAXS intensity profiles along q_y. Spectra for incident angles of 0.1° and 0.05° are also shown, shifted vertically for clarity. The horizontal lines in (a) and (c) indicate the locations of the spectra in (c), (d). The arrows indicate the scattering peaks corresponding to the Bragg reflections arising from cylinder-like structures.

on the ALD deposition temperature, as shown in Fig. 6b. Annealing at higher temperatures sharpened the WAXS peaks. Using the Scherrer equation, crystallite sizes of 13 nm for 250 °C and 350 °C, and 25 nm for 450 °C were found. While a detailed study of the ZnO crystallisation kinetics is outside the scope of this study, the increase of crystallise size in the BCP confinement with annealing temperature mirrors the results obtained for TiO_2, where the crystallite size increased with increasing annealing temperature (400-700 °C) from 12 nm to 28 nm.[29] Crystallite sizes in the 20 nm range were reported to optimize performance in hybrid solar cells.[30]

While the structural characterization of replicated gyroids has been carried out before,[3] less is known about the wormlike morphology. Figure 7a shows grazing incidence small angle scattering (GISAXS) spectra of a voided wormlike polystyrene template. This spectrum shows structure at lateral positions which correspond to a lattice spacing of

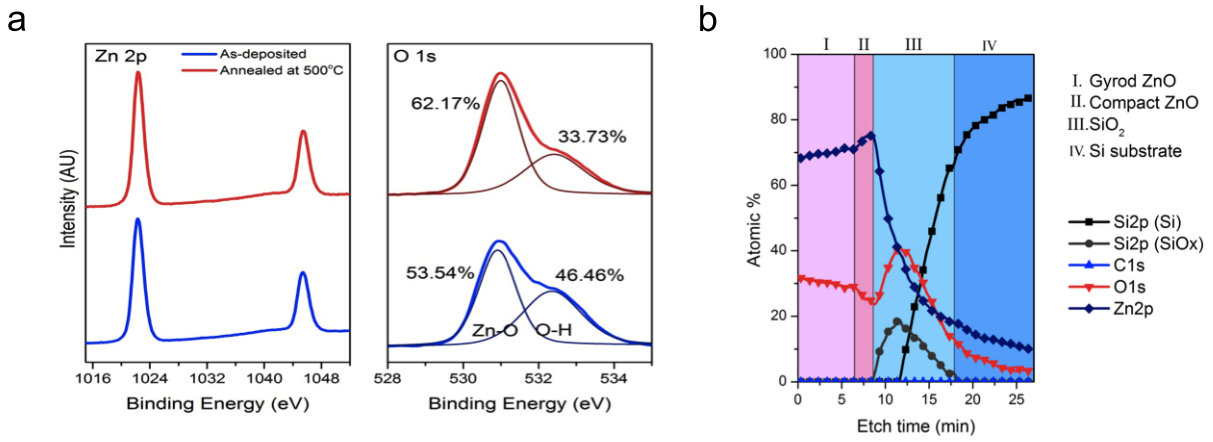

Figure 8: XPS spectra of (a) Zn 2p and O 1s on as-deposited and annealed films. (b) Depth profile of annealed film.

≈ 57 nm. These are quantified by the 1D intensity profile in Fig. 7b that was extracted along q_y and averaged over the q_z-range where the transmission function of the polymer film has a maximum. Lorentz functions were fitted to the three scattering peaks that correspond to three orders of Bragg reflections arising from the pore morphology in the film. The three reflections have q ratios of $1 : \sqrt{4} : \sqrt{7}$, which is characteristic for a hexagonally packed assembly of cylinder segments. The Bragg rods are bent inwards, which we attribute to tilting of the cylinder segments away from a fully perpendicular orientation, i.e. the scattering signal arises from randomly oriented cylinders. The presence of higher orders Bragg reflections points to the formation of this locally symmetric randomly oriented morphology within the entire film.

The GISAXS spectrum in Fig. 7c of the ALD ZnO replica shows lateral Bragg reflections at positions which correspond to lattice spacing of ≈ 63 nm. Figure 7d shows the q_z-averaged 1D intensity profile along q_y at maximal transmission function (bottom), together with the profile extracted at $q_z \approx 0.053$ Å^{-1} (2$^{\text{nd}}$ from bottom). The Bragg rods at $q_y = 2\pi/d_{\text{cyl}}$ are vertical, which is indicative of laterally ordered cylinder segments. The scattering features at $q_z \approx 0.053$ Å^{-1} can be attributed to cylinder segments distributed along q_z, i.e. the cylinder spacing is not constant along q_z (with a periodic variation of a few nm) or the cylinder segments are slightly tilted. This observation is further supported by the presence of the first and third order Bragg peaks, with a missing second order reflection (bottom curve). This points to an asymmetry of the cylinder structure, which is particularly pronounced at the interface with the substrate.

The ZnO film was additionally probed at further two incident angles of 0.1° and 0.05°, which give information on the morphology close to the film surface. These spectra do not show the cylinder asymmetry and the variation of the Bragg rods along q_z is also absent in the 2D GISAXS spectra (see Supporting Information).

2.1.5 X-ray photoemission spectroscopy (XPS)

The chemical composition of the film was probed by XPS . Figure 8a shows the Zn 2p and O 1s spectra of as-deposited and 400 °C annealed films. The Zn 2p3 peak appears at 1022.4 eV, in good agreement with previous reports for ZnO.[31] The O 1s peak can be deconvoluted into a low binding energy peak at 530.9 eV and a high binding energy peak at 532.4 eV. The low binding energy peak is assigned to fully coordinated Zn-O-Zn oxygen atoms, while the high binding energy peak arises from partly coordinated Zn-O-H atoms. The percentages are the relative contribution of each peak, showing that annealing increases the percentage of fully coordinated O atoms in the film. The surface scan also revealed the existence of adventitious carbon (not shown here) which accounted for $\sim 10\%$ of the atomic composition.

A XPS profile measured the composition of the mesoporous material across the thickness of the film. Figure 8b shows the variation of the Zn 2p, O 1s, C 1 and Si 2p (Si and SiO_2) signals with etching time. The spectrum of the top surface in Fig. 8a was not included in the depth profile because of the 10% carbon contamination. The depth profile shows that the composition of the ZnO gyroid (I) is uniform up to the ZnO compact layer (II) on the SiO_2/Si substrate (III and IV). Additionally, this result shows that that the mesoporous layer is carbon-free, demonstrating the full removal of the polymer template. ZnO composition throughout the film is not stochiometric but highly oxygen deficient, as expected for a ZnO layer.

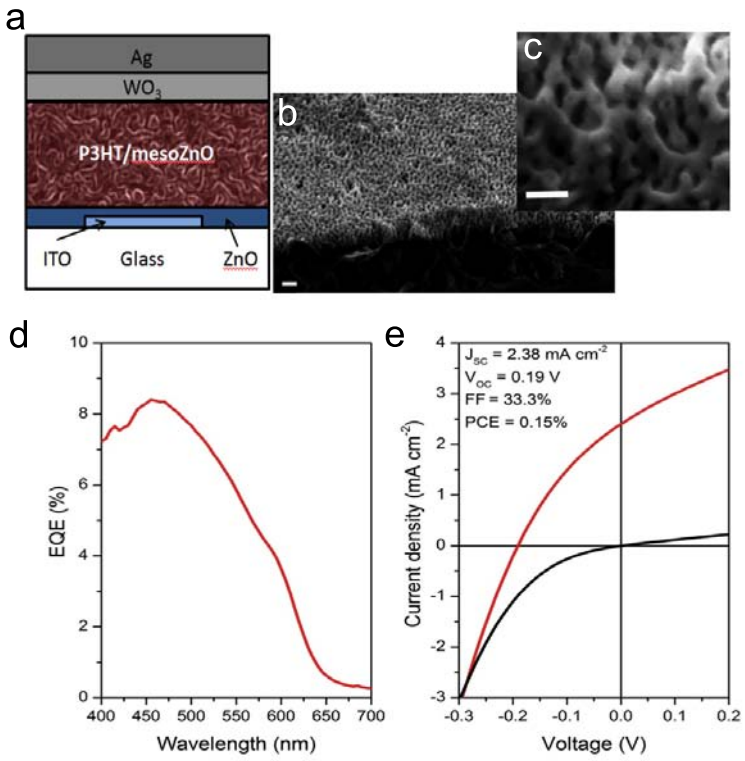

Figure 9: Summary of the architecture and performance of a ZnO/P3HT device built using a wormlike ZnO film of 250 nm thickness. (a) Schematics of the deice (b), (c) SEM images of the wormlike ZnO layer in two magnifications. The scale bars correspond to 100 nm. (d) External qantum efficiency and (e) current-voltage characteristic of the device. The lower line shows the performance of a ZnO/P3HT bilayer device.

2.1.6 Hybrid photovoltaic cell

To demonstrate the potential of application of the ALD-generated mesoporous ZnO layer for hybrid photovoltaics, a polymer/mesoZnO solar cell was fabricated. For this purpose, a wormlike mesoporous layer was deposited onto a conductive pre-patterned ITO substrate and infiltrated with poly(3-hexylthiophene) (P3HT) polymer. The wormlike ZnO structure was chosen because, we have better control over film thickness and uniformity compared to the gyroid template. Figure 9 a and b show the external quantum efficiency (EQE) of the photovoltaic device and its current-voltage ($J-V$) characteristic under solar-simulator illumination, respectively. The device performance parameters including the short circuit current $J_{\rm sc}$, the open circuit voltage $V_{\rm oc}$, the fill factor FF, and the power conversion efficiency PCE are shown in the inset of Fig. 9b.

The short circuit current of the device ($J_{\rm sc} = 2.38\,{\rm mA/cm^2}$) is significantly improved compared to a bilayer device comprised of non-porous ZnO and P3HT ($J_{\rm sc} = 0.47\,{\rm mA/cm^2}$)) in the otherwise same device architecture.[32] The increased effective surface area in the mesoporous layer increases exciton dissociation at the ZnO/P3HT interface and hence increases the photocurrent. The open circuit voltage ($V_{\rm oc}$) of the ZnO/P3HT couple depends on the ZnO work function and the bandgap. The value of $V_{\rm oc} = 0.19\,{\rm V}$ of our device is much below $V_{\rm oc} = 0.43\,{\rm V}$ that was found in of P3HT/ZnO nanowire devices.[28] This reduced value of $V_{\rm oc}$ points to the existence of sub-bandgap states on the ZnO surface, which may arise from a surface chemistry that differs from bulk ZnO. Further optimization of the ALD generated ZnO is required to increase the open-circuit voltage of the device. Finally, the relatively low fill factor (FF) of the device suggests that charges are not extracted efficiently from the device. This might either be due to resistance within the mesoporous structure and/or connectivity the solid ZnO and/or WO_3 blocking layers. It is is likely that the main cause limiting the fill factor is the lack of control of the surface roughness during the ICP etching of the compact layer. Further studies aiming to improve $V_{\rm oc}$ and FF are ongoing. Given the scope for optimization, the results of Fig. 9 are promising. Note that ZnO-polymer hybrid solar cells typically have power conversion efficiencies

below 1%,[33] and that the performance of our photovoltaic device is comparable to previous reports of P3HT/ZnO nanocrystal mesoporous layers.[30]

3 Conclusions

ALD deposition of ZnO into a nanoporous polymer matrix allows the fabrication of well-defined, 3D ZnO scaffolds with 20-40 nm wide struts. While similar morphologies of other metal oxides have been created using a range of deposition techniques, the controlled manufacture of 3D interconnected ZnO skeletons is remarkable because the low crystallization temperature of ZnO makes the molding of ZnO into design morphologies very difficult.

Two different morphologies based on the self-assembly of a PS-PI block-copolymer are presented. The carefully annealed polymer phase morphology leads to the highly periodic double gyroid morphology, while a wormlike morphology was observed upon rapid quenching. Both morphologies consisted of a well-defined strut-network with interconnected pores. While the highly periodic ZnO gyroid is conceptionally attractive, it requires delicate processing and a longer preparation time. The wormlike structure, on the other hand, is robust to generate and more controllable, which could be beneficial for production at a larger scale.

The key for the realization of these structures is to bypass the rapid crystallization of ZnO during material deposition. Since the ALD principle relies on surface limited reactions leading to the conformal coating of a 3D surface, good control over the surface chemistry of the mould is imperative. For the present system, this implies a dense coverage of the pore surface with OH groups. Because of the pore size of only 30 nm, this requirement is especially stringent since the formation of even the smallest crystallites leads to pore blockage.

The fabricated films were characterized using XPS, WAXS, GISAXS and SEM, which confirmed deposition of wurtzite ZnO throughout the film. The as-deposited ZnO (at 80 °C) onto the polymer substrate was (partially) nanocrystalline, and crystallites grew larger upon post annealing at high temperatures. The structure showed thermal stability up to 550 °C. The average pore width of approximately 30 nm is ideal for exciton dissociation in hybrid photovoltaic devices. Preliminary results of a P3HT/ZnO device based on the wormlike morphology demonstrate the promise of this material for photovoltaic applications.

The manufacture of a ZnO based solar cell showed the feasibility of the integration of the 3D mesostructured ZnO networks into devices. More promising than the direct function of ZnO in photovoltaics is its use electrode material in solar cells,[34,35] in organic LEDs and lasers, and as highly sensitive gas sensors.[36]

4 Experimental

Template fabrication:[18,19] The polymers used for template fabrication were polystyrene (45 kg/mol) - *block* - polyisoprene (39 kg/mol), purchased from Polymer Source Inc., Canada, and polystyrene (10 kg/mol), purchased from Sigma Aldrich. PS-*b*-PI and PS were mixed to result in 65% volume fraction of PS and dissolved in toluene. For the self-assembled gyroid structure, 20 µl of solution was drop-cast onto a substrate (Si, ITO, or glass) of 1.2 cm × 1.2 cm. A PTFE film of 1 cm × 1 cm was placed onto the middle of the drop and the film was placed into a sealed chamber containing toluene vapor at 4 °C for up to 7 days. For the wormlike morphology, 60 µl of the mixed polymer solution was spin coated onto a substrate at 1000 rpm for 90 seconds. The film was then taken out of the chamber and left in air at room temperature for an additional 24 hours before exposure to UV light (254 nm) for 12 hours in order to degrade the polyisoprene block. The degradation product was then removed by placing the film in ethanol solution for 15 hours. In order to minimize peeling and cracking of the film, the sample was placed upside down on a lint-free tissue and dried.

ZnO replication: A Beneq TFS200 system was used for ALD. The ZnO precursors were diethyl zinc $(C_2H_5)_2Zn$, purchased from ABCR GmbH, and deionized water (H_2O). Between 65 and 250 deposition cycles were used. The optimized protocol for continuous flow method consisted of pulse/purge times of 30 s for the first 30 cycles, 1 min for the following 40 cycles, and 2 min for the last 30 cycles. A typical half cycle in the stop-flow method consisted of a 10 s pulse followed by 1 min hold time with the vacuum and nitrogen flow off, followed by a 1 min purge time. ZnO deposition was normally carried out at 80 °C, but depositions at 100 °C and 120 °C were also made for comparison. The ALD parameters of the samples shown in the figures are summarized in Table 1.

Removal of PS template: The deposited ZnO-polymer hybrid was exposed to either an oxygen plasma (Diener Plasma Etcher) or calcination at temperatures above 400 °C. Depending on the thickness of the mesoporous template, a plasma duration 15 to 45 min was required. High temperature removal of PS was achieved by heating (10 °C/minute) to a temperature above 450 °C followed by annealing for 2 hours in air.

Removal of the of compact ZnO top layer: An Oxford Instrument inductively coupled plasma etcher was used to etch-off the top nonporous ZnO layer that has formed by ALD. 6 min of etching removed the 30 nm ZnO. The etchant gases were CHF_3 (50 ccm) and Ar (25 ccm) using an RF power of 100 W and a forward power 1550 W.
X-ray Diffraction: Wide angle x-ray scattering measurements, were carried out using a Bruker D8 diffractometer. The samples were prepared on a Si substrate. Grazing- incidence small-angle scattering (GISAXS) measurements were performed at beamline P03[37](PETRA III), HASYLAB at DESY in Hamburg, Germany. At P03 the wavelength was 1.09 Å. The beam was focused by beryllium compound refractive lenses to a size of 31 µm × 22 µm (horizontal × vertical) at the sample position, with an incident angle of 0.185° for the polystyrene template, and 0.05°, 0.1° and 0.2° for the resulting ZnO film. A Pilatus 1M area detector was used for the detection of the scattered intensity. The pixel sizes were 172 µm × 172 µm. The sample-detector distances were 4.260 m for polystyrene and 3.651 m for ZnO. The sample was moved out of the beam after each measurement to avoid beam damage. The q-space calibration was performed fitting the characteristic scattering signal arising from 400 nm colloids. The conversion of the 2D images from pixels to q-values as well as the construction of 1D profiles and the peak fitting were carried out using a self-written GISAXS Igor Pro analysis package.
X-ray photoemission spectroscopy measurements: The gyroid ZnO samples were fabricated on an oxide covered silicon wafer which was transferred into the ultrahigh vacuum chamber of a ESCALAB 250Xi for XPS measurements. The measurements were carried out using a XR6 monochromated Alkα X-ray source ($h\nu = 1486.6$ eV) with a 650 µm spot size. For the XPS depth profiling, the sample was etched using an Ar^+ ion beam with an energy of 3000 eV.
Photovoltaic device fabrication: A worm-like ZnO mesoporous film was fabricated on a prepatterned ITO/glass substrate as described above. Poly(3-hexylthiophene) (P3HT) (from Reike Metals) polymers were dissolved in anhydrous chlorobenzene and spin-coated onto the ZnO mesoporous layer. The samples were then transferred into a thermal evaporation chamber for WO_3 (10 nm), Ag (30 nm), and Al (60 nm) deposition under high vacuum (10^{-6} mbar). Finally, the devices were post-annealed at 140 °C for 10 min.
Photovoltaic performance characterization: For external quantum efficiency (EQE) measurements (in air) a 250 W tungsten halogen lamp and an Oriel Cornerstone 130 monochromator were used. The measurements were performed as a function of wavelength at an intensity of $\sim 1\,\mathrm{mW/cm^3}$. To measure the $J-V$ curve of the device under AM1.5 conditions, an ABET Solar 2000 solar simulator was used. In order to obtain reliable data, a spectral mismatch correction was carried out using a calibrated and certified inorganic solar cell.

1. Djurišić, A.B., Chen, X., Leung, Y.H., and Ng, A.M.C. (2012) ZnO nanostructures: growth, properties and applications. *J. Mater. Chem.*, **22** (14), 6526.
2. Gwinner, M.C., Vaynzof, Y., Banger, K.K., Ho, P.K.H., Friend, R.H., and Sirringhaus, H. (2010) Solution-processed zinc oxide as high-performance air-stable electron injector in organic ambipolar light-emitting field-effect transistors. *Adv. Funct. Mater.*, **20** (20), 3457–3465.
3. Crossland, E., Kamperman, M., Nedelcu, M., Ducati, C., Wiesner, U., Smilgies, D., Toombes, G., Hillmyer, M., Ludwigs, S., and Steiner, U. (2008) A bicontinuous double gyroid hybrid solar cell. *Nano Letters*, **9** (8), 2807–2812.
4. Zhang, Q., Dandeneau, C.S., Zhou, X., and Cao, G. (2009) ZnO nanostructures for dye-sensitized solar cells. *Adv. Mater.*, **21** (41), 4087–4108.
5. Qiu, J., Guo, M., and Wang, X. (2011) Electrodeposition of hierarchical ZnO nanorod-nanosheet structures and their applications in dye-sensitized solar cells. *ACS Applied Materials & Interfaces*, **3** (7), 2358–2367.
6. Ko, S., Lee, D., Kang, H., Nam, K., Yeo, J., Hong, S., Grigoropoulos, C., and Sung, H. (2011) Nanoforest of hydrothermally grown hierarchical ZnO nanowires for a high efficiency dye-sensitized solar cell. *Nano Letters*, **11** (2), 666–671.
7. Scharrer, M., Wu, X., Yamilov, A., and Cao, H. (2005) Fabrication of inverted opal zno photonic crystals by atomic layer deposition. *Appl. Phys. Lett.*, **86** (15), 151 113. URL `http://link.aip.org/link/?APPLAB/86/151113/1`.
8. Wagner, T., Waitz, T., Roggenbuck, J., Fröba, M., Kohl, C.D., and Tiemann, M. (2007) Ordered mesoporous ZnO for gas sensing. *Thin Solid Films*, **515** (23), 8360–8363.
9. Lepoutre, S., Julián-López, B., Sanchez, C., Amenitsch, H., Linden, M., and Grosso, D. (2010) Nanocasted mesoporous nanocrystalline ZnO thin films. *J. Mater. Chem.*, **20** (3), 537.
10. Hashimoto, T., Nishikawa, Y., and Tsutsumi, K. (2007) Identification of the "voided double-gyroid-channel": A new morphology in block copolymers. *Macromolecules*, **40** (4), 1066–1072.
11. Crossland, E., Cunha, P., Scroggins, S., Moratti, S., Yurchenko, O., Steiner, U., Hillmyer, M., and Ludwigs, S. (2010) Soft-etch mesoporous hole-conducting block copolymer templates. *ACS Nano*, **4** (2), 962–966.
12. Yang, P., Zhao, D., Margolese, D.I., Chmelka, B.F., and Stucky, G.D. (1999) Block copolymer templating syntheses of mesoporous metal oxides with large ordering lengths and semicrystalline framework. *Chem. Mater.*, **11**, 2813–2826.

13. Hsueh, H. and Ho, R. (2012) Bicontinuous ceramics with high surface area from block copolymer templates. *Langmuir*, **28** (22), 8518–8529.

14. Gordon, R., Hausmann, D., Kim, E., and Shepard, J. (2003) A kinetic model for step coverage by atomic layer deposition in narrow holes or trenches. *Chemical Vapor Deposition*, **9** (2), 73–78.

15. Karuturi, S.K., Liu, L., Su, L.T., Chutinan, A., Kherani, N.P., Chan, T.K., Osipowicz, T., and Tok, A.I.Y. (2011) Gradient inverse opal photonic crystals via spatially controlled template replication of self-assembled opals. *Nanoscale*, **3** (12), 4951.

16. Elam, J., Routkevitch, D., Mardilovich, P., and George, S. (2003) Conformal coating on ultrahigh-aspect-ratio nanopores of anodic alumina by atomic layer deposition. *Chem. Mater.*, **15** (18), 3507–3517.

17. Wang, Y., Qin, Y., Berger, A., Yau, E., He, C., Zhang, L., Gösele, U., Knez, M., and Steinhart, M. (2009) Nanoscopic morphologies in block copolymer nanorods as templates for atomic-layer deposition of semiconductors. *Adv. Mater.*, **21** (27), 2763–2766.

18. Finnemore, A.S., Scherer, M.R.J., Langford, R., Mahajan, S., Ludwigs, S., Meldrum, F.C., and Steiner, U. (2009) Nanostructured calcite single crystals with gyroid morphologies. *Adv. Mater.*, **21** (38â39), 3928–3932.

19. Scherer, M. (2009) *Nanostructured Materials via Self-Assembled Templates*, Master's thesis, University of Konstanz.

20. Ndoni, S., Li, L., Schulte, L., Szewczykowski, P.P., Hansen, T.W., Guo, F., Berg, R.H., and Vigild, M.E. (2009) Controlled photooxidation of nanoporous polymers. *Macromolecules*, **42** (12), 3877–3880.

21. Yamada, A., Sang, B., and Konagai, M. (1997) Atomic layer deposition of zno transparent conducting oxides. *Applied surface science*, **112**, 216–222.

22. Grigoras, K., Airaksinen, V., and Franssila, S. (2009) Coating of nanoporous membranes: atomic layer deposition versus sputtering. *J. Nanosci. Nanotechnol.*, **9** (6), 3763–3770.

23. Guldin, S., Docampo, P., Stefik, M., Kamita, G., Wiesner, U., Snaith, H.J., and Steiner, U. (2012) Layer-by-layer formation of block-copolymer-derived TiO_2 for solid-state dye-sensitized solar cells. *Small*, **8**, 432–440.

24. George, S. (2010) Atomic layer deposition: an overview. *Polymer*, **1550**, 125.

25. Skoog, S., Bayati, M., Petrochenko, P., Stafslien, S., Daniels, J., Cilz, N., Comstock, D., Elam, J., and Narayan, R. (2012) Antibacterial activity of zinc oxide-coated nanoporous alumina. *Mat. Sci. Eng. B*, **117**, 992–998.

26. Alessandri, I., Zucca, M., Ferroni, M., Bontempi, E., and Depero, L. (2009) Growing zno nanocrystals on polystyrene nanospheres by extra-low-temperature atomic layer deposition. *Crystal Growth and Design*, **9** (3), 1258–1259.

27. Urbas, A., Maldovan, M., DeRege, P., and Thomas, E. (2002) Bicontinuous cubic block copolymer photonic crystals. *Adv. Mater.*, **14** (24), 1850–1853.

28. Olson, D., Shaheen, S., Collins, R., and Ginley, D. (2007) The effect of atmosphere and ZnO morphology on the performance of hybrid poly (3-hexylthiophene)/zno nanofiber photovoltaic devices. *The Journal of Physical Chemistry C*, **111** (44), 16 670–16 678.

29. Guldin, S., Hüttner, S., Tiwana, P., Orilall, M., Ülgüt, B., Stefik, M., Docampo, P., Kolle, M., Divitini, G., Ducati, C., Redfern, S., Snaith, H., Wiesner, U., Eder, D., and Steiner, U. (2011) Improved conductivity in dye-sensitised solar cells through block-copolymer confined TiO_2 crystallisation. *Energy & Environmental Science*, **4**, 225–233.

30. Boucle, J., Snaith, H., and Greenham, N. (2010) Simple approach to hybrid polymer/porous metal oxide solar cells from solution-processed ZnO nanocrystals. *The Journal of Physical Chemistry C*, **114** (8), 3664–3674.

31. Ehrler, B., Musselman, K.P., Böhm, M.L., Morgenstern, F.S., Vaynzof, Y., Walker, B.J., MacManus-Driscoll, J.L., and Greenham, N.C. (2013) Preventing interfacial recombination in colloidal quantum dot solar cells by doping the metal oxide. *ACS Nano*, p. DOI: 10.1021/nn400656n.

32. Vaynzof, Y., Kabra, D., Zhao, L., Ho, P., Wee, A., and Friend, R. (2010) Improved photoinduced charge carriers separation in organic-inorganic hybrid photovoltaic devices. *Appl. Phys. Lett.*, **97** (3), 033 309.

33. Li, F., Chen, W., Yuan, K., and Chen, Y. (2012) Photovoltaic performance enhancement in P3HT/ZnO hybrid bulk-heterojunction solar cells induced by semiconducting liquid crystal ligands. *Organic Electronics*, **12** (11), 2757–2762.

34. Sun, Y., Seo, J.H., Takacs, C.J., Seifter, J., and Heeger, A.J. (2011) Inverted polymer solar cells integrated with a low-temperature-annealed sol-gel-derived ZnO film as an electron transport layer. *Adv. Mater.*, **23**, 1679–1683.

35. You, J., Dou, L., Yoshimura, K., Kato, T., Kenichiro Ohya and, T.M., Emery, K., Chen, C.C., Gao, J., Li, G., and Yang, Y. (2013) A polymer tandem solar cell with 10.6% power conversion efficiency. *Nature Communicaitons*, **4** (1446), 1446.

36. Schmidt-Mende, L. and MacMagnus-Driscoll, J.L. (2007) Zno-nanostructures, defects, and devices. *Materials Today*, **10** (5), 40–48.

37. Buffet, A., Rothkirch, A., Dohrmann, R., Körstgens, V., Abul Kashem, M.M., Perlich, J., Herzog, G., Schwartzkopf, M., Gehrke, R., Müller-Buschbaum, P., and Roth, S.V. (2012) P03, the microfocus and nanofocus x-ray scattering (MiNaXS) beamline of the PETRA III storage ring: the microfocus endstation. *J Synchrotron Radiat.*, **19** (4), 647–653.

Acknowledgements The authors thank S. Vignolini for her invaluable help and P. Müller-Buschbaum for providing the GISAXS beamtime. We acknowledge Nokia Research Centre (Cambridge, UK) and the EPSRC for funding. Parts of this research were carried out at the light source PETRA III at DESY. DESY is a member of the Helmholtz Association (HGF).